ATMOSPHERIC SCIENCE LETTERS
Atmos. Sci. Let. (2014)
Published online in Wiley Online Library
(wileyonlinelibrary.com) **DOI:** 10.1002/asl2.533

RMetS
Royal Meteorological Society

Universal evolution mechanisms and energy conversion characteristics of long-lived mesoscale vortices over the Sichuan Basin

Shenming Fu,[1]* Wanli Li,[2] Jianhua Sun,[3] Jingping Zhang[4] and Yuanchun Zhang[3]

[1]*International Center for Climate and Environment Sciences, Institute of Atmospheric Physics, Chinese Academy of Sciences, Beijing, China*
[2]*China Meteorological Administration Training Center, Beijing, China*
[3]*Key Laboratory of Cloud-Precipitation Physics and Severe Storms, Institute of Atmospheric Physics, Chinese Academy of Sciences, Beijing, China*
[4]*Department of Atmospheric Sciences, Nanjing University of Information Science and Technology, China*

*Correspondence to:
S. Fu, International Center for Climate and Environment Sciences, Institute of Atmospheric Physics, Chinese Academy of Sciences, Beijing 100029, China.
E-mail: fusm@mail.iap.ac.cn

Received: 6 May 2014
Revised: 10 August 2014
Accepted: 13 August 2014

Abstract

The mesoscale southwest vortices (SWVs) over the Sichuan Basin during the summer of 2000–2013 were detected and tracked based on a high-resolution reanalysis data and station observations. Four types of SWV were classified according to dynamical and thermodynamical standards, and their main features were compared. This study presents the first analysis of the universal evolution mechanisms and energy conversion characteristics of long-lived SWVs by using the vorticity and kinetic energy budgets, as well as a new composite method under a normalized polar coordinate. Also, this study is the first work to reveal the three-dimensional shape of SWVs.

Keywords: **mesoscale vortex; vorticity budget; energy conversion**

1. Introduction

In summer, mesoscale vortex is one of the most important triggers for torrential rain events over the Yangtze River Basin (YRB) (Tao, 1980; Zhao *et al.*, 2004), particularly for those extreme heavy rainfall cases that last several days and cause flash floods (Kuo *et al.*, 1988). There are two main mesoscale vortex sources over the YRB (Yang *et al.*, 2010): the first is near the Sichuan Basin (Figure 1(a)) and the second is around the Dabie Mountain. The mesoscale vortex originating near the Sichuan Basin is referred to as the southwest vortex (SWV) by Chinese meteorologists (Kuo *et al.*, 1988). The SWV is a type of meso-α vortex (Orlanski, 1975; Figure 1(b) and (c)) that is mainly detected in the lower troposphere (Lu, 1986). Most of the SWVs maintain quasistationary behavior (Chen *et al.*, 2007); however, under strong steering flow, some SWVs can move out of the Sichuan Basin and cause series of heavy rainfall events along their track that significantly increases the risk of flooding over the YRB (Zhao *et al.*, 2004).

Owing to its great importance, the SWV has been the focus of many studies. Their synoptic environmental conditions (Lu, 1986), three-dimensional structure (Zhao *et al.*, 2004), convection activities (Kuo *et al.*, 1988), and evolution mechanisms (Fu *et al.*, 2013) were widely discussed. However, thus far, most of these studies are case studies; therefore, universal features of the SWV are still vague. It should be noted that although there are some statistical and climatological analyses that focused on the generality of the SWV (Lu, 1986; Chen *et al.*, 2007), the classification criteria of SWVs were mainly based on the vortex sources and/or whether the SWV can move out of the Sichuan Basin; moreover, no dynamical diagnosis had been applied in these studies, therefore, universal features during the evolution and energy conversion processes of the SWV remain unclear. On the basis of the previous studies, the purpose of this study is to conduct statistical and composite studies of the SWVs with a new criterion and to show the universal evolution and energy conversion features of the long-lived SWVs.

2. Data and method

2.1. Data

Six-hourly climate forecast system (CFS) reanalysis data (Saha *et al.*, 2010) with a resolution of $0.5 \times 0.5°$ from the National Centers for Environmental Prediction (NCEP) during the summer, from June to August, of 2000–2013 were used to detect the SWVs and calculate the budgets. Routine surface observation and soundings from the Chinese Meteorological Administration (CMA) were used to validate the detected SWVs, and the observational data were also used in the SWV classification.

2.2. Detection and estimation of the SWV size characteristics

In this study, an SWV's initiation is defined as the first detection of a closed center at the stream field (700 hPa) coupled with a remarkable positive vorticity

center within (26–34°N, 103–110°E). The SWV was validated if the observed wind (from surface to 700 hPa) surrounding the detected SWV center is characterized by significant cyclonic shear. Lifespan of the SWV is defined as the period between the first and last detection of the same SWV. After detecting an SWV, vertical stretching of the vortex was examined by determining the continuous vertical levels also with significant vortex circulations. Additionally, the distance between the vortex centers at neighboring levels should be less than 50 km.

The method from Rudeva and Gulev (2007, 2011) was utilized to estimate the SWV size features. Main procedures are as follows: (1) for each time step, transform the original coordinate system by collocating the SWV center with the center of the polar coordinate system; (2) interpolate potential vorticity (PV) onto the 36 radii (0° represents east, with a 10° angular step) relative to the vortex center; (3) along all 36 radii, calculate $\partial \mathrm{PV}/\partial r = -0.001$ potential vorticity unit (PVU)/km, where a first guess radius and a critical PV value are determined; and (4) determine the minimum of the 36 critical PV values and interpolate locations of the minimum critical PV along all other radii to determine the critical positions. Therefore, a curve M connecting all 36 critical positions can be determined. After calculating the area S_M surrounded by the curve M, the vortex effective radius r_{ef} is calculated as $r_{\mathrm{ef}} = \sqrt{S_M/\pi}$.

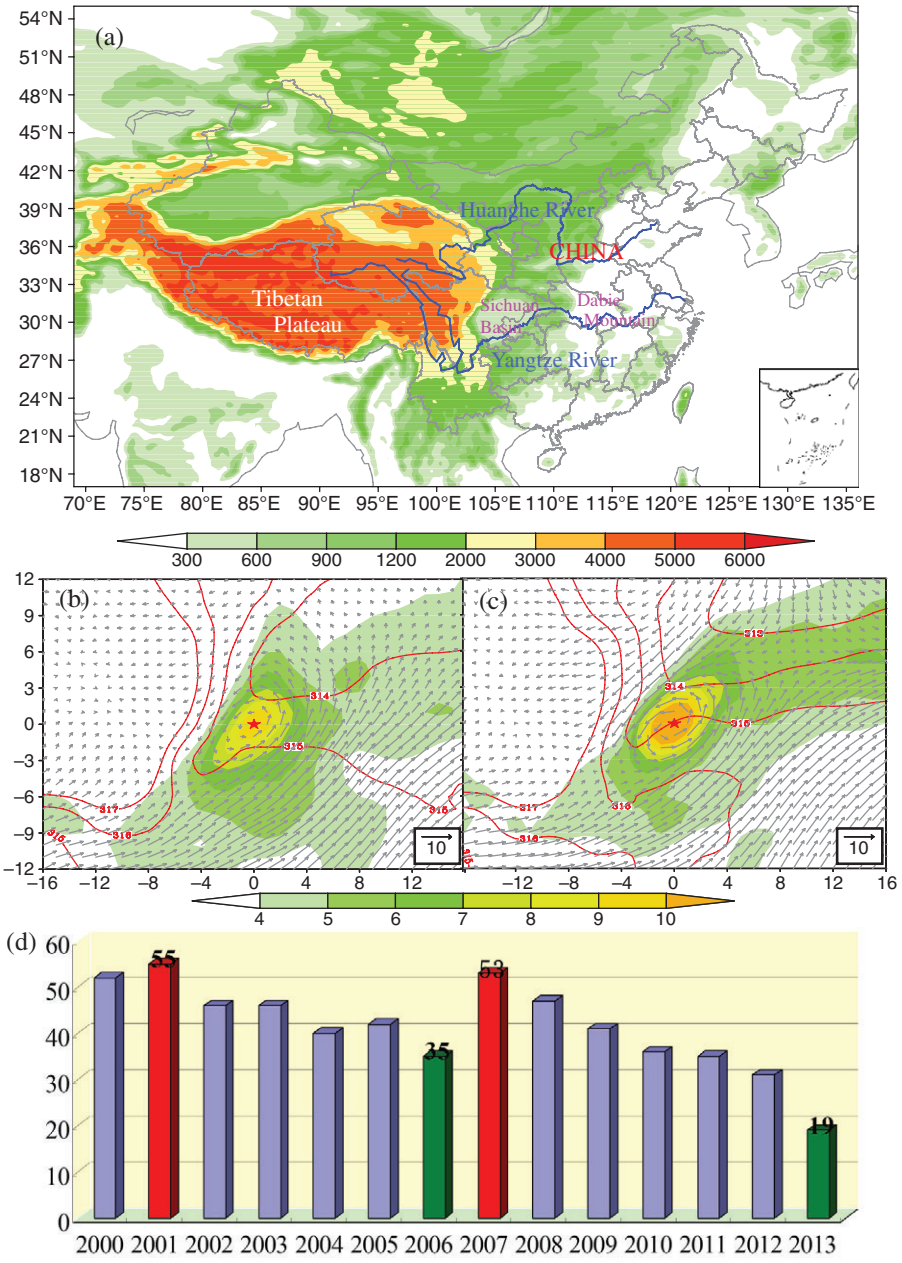

Figure 1. (a) Topography (shaded, units: m) of the Sichuan Basin, (b) composed PN-SWV, and (c) PL-SWV during the developing stage, where the shaded is PV (units: 0.1 PVU), red solid lines indicate potential temperature (units: K), and the gray vector represents horizontal wind field (units: m s^{-1}). The ordinate and abscissa in (b) and (c) represent the grid point relative to the composed vortex center, and the grid spacing is 50 km. (d) Annual frequency of SWVs.

To compose the SWVs, a normalization of radius was applied to all radii: $r_{ni} = r_{oi}/R_i$, where r_{ni} is the normalized position along the ith azimuth corresponding to its original position r_{oi}, and R_i is the critical radius along that azimuth. Budget terms at typical stages were composed under the normalized polar coordinate. Complete descriptions of this method have been reported by Rudeva and Gulev (2007, 2011).

2.3. Vorticity and energy conversion budget method

The vorticity budget equation from Kirk (2003) was used in this study:

$$\frac{\partial \zeta}{\partial t} = \mathrm{HAV} + \mathrm{VAV} + \mathrm{TIL} + \mathrm{STR} + \mathrm{RES} \qquad (1)$$

where ζ is the vertical vorticity, HAV is the horizontal advection of vorticity, VAV is the vertical advection of vorticity, TIL represents the titling effect, STR denotes the stretching effect, and RES stands for the residual term. Additionally, the total effect was defined as TOT = HAV + VAV + TIL + STR.

Kinetic energy (KE) budget equations of the rotational and divergent wind (Ding and Liu, 1985; Fu *et al.*, 2011) were used in this study:

$$\frac{\partial K_\psi}{\partial t} = B_\psi + H\left(K_\chi, K_\psi\right) + F_\psi \qquad (2)$$

$$\frac{\partial K_\chi}{\partial t} = B_\chi + H\left(P, K_\chi\right) - H\left(K_\chi, K_\psi\right) + F_\chi \qquad (3)$$

$$\frac{\partial (P+I)}{\partial t} = B_{P+I} - H\left(P, K_\chi\right) + Q_{P+I} + F_{p+I} \qquad (4)$$

where ψ and χ are the stream and potential function, respectively. K_ψ and K_χ are rotational and divergent wind KE, respectively. $P+I$ is the total potential energy, where P is the potential energy and I is the internal energy. B_ψ, B_χ, and B_{P+I} are the boundary fluxes; F_ψ, F_χ, and F_{p+I} are the residual terms of Equations (2)–(4), respectively; and Q_{P+I} represents the diabatic process.

Term $H(P, K_\chi)$ denotes the conversion between available potential energy (APE) and divergent wind KE, which represents the baroclinic energy conversion (BCC). Term $H(K_\chi, K_\psi)$ denotes the transition between divergent wind KE and rotational wind KE, which represents the barotropical energy conversion (BTC).

3. Results

3.1. Overview of the statistical results of SWVs

A total of 578 SWVs were detected during the study period (Figure 1(d)), and only 139 (24.1%) of them spanned a lifetime more than 12 h. On the basis of the 3-hourly surface observation, SWVs maintained more than 12 h were classified according to both dynamical and thermodynamical standards (James and Johnson, 2010), with the respective criteria of whether a surface low center appeared and whether obvious precipitation occurred within 6 h before the formation of the SWV. Therefore, four types of SWV were determined, including the no precipitation no surface low type (NN), the only precipitation type (PN), the only surface low type (NL), and the both precipitation and surface low type (PL). Classification results are shown in Table I, which indicate that the PL and PN types accounted for 82.7% of the total number, spanning a much longer lifetime, causing much more intense precipitation, and stretched thicker vertical levels than the other two types. Moreover, the PL-SWV was generally more intense than the PN-SWV, except for the three-dimensional shape (Tables I and II). Therefore, the initial conditions including the thermodynamical processes associated with precipitation and dynamical processes associated with the surface low center are vital in determining the features of SWVs.

The vertical stretching of all four types of SWVs (Table I) reveals that the SWV is located mainly in the middle and lower troposphere rather than only the lower troposphere, and its central level is approximately 700 hPa. Additionally, composite results of vorticity (not shown) reveal that 700 hPa was the closest level to the maximum positive vorticity level. Therefore, 700 hPa was selected as the typical level in this study.

Previous studies (Lu, 1986; Chen *et al.*, 2007) reveal that an SWV with a lifetime more than 36 h can be defined as long-lived. Therefore, 36 h was used as the threshold value in this study. Among all 139 SWVs, only 30 cases (21.6%) maintained for more than 36 h, including 15 PN- and 15 PL-SWVs; all NN- and

Table I. Statistical results of the SWVs with life spans of more than 12 h, including the number and percentage of each type of SWV (NAP), the averaged life span (ALS), maximum 6-h precipitation during the SWV lifetime (MP), the averaged uppermost stretching level (AUS), and the averaged lowermost stretching level (ALS).

	NN	PN	NL	PL	Total
NAP (%)	13 (9.4%)	71 (51.1%)	11 (7.9%)	44 (31.6%)	139 (100%)
ALS (h)	20.3	27.6	21.8	30.7	27.5
MP (mm)	5.5	44.1	19.4	55.8	42.1
AUS (hPa)	608	561	590	570	569
ALS (hPa)	823	865	831	874	861

Table II. Effective radius (units: km), vortex-averaged vorticity budget terms (units: $10^{-10}\,s^{-2}$), as well as vortex-averaged baroclinic and barotropical energy conversions (units: 10^{-4} W kg^{-1}) during typical stages of the composed PN-SWV (without parentheses) and PL-SWV (with parentheses).

	HAV	VAV	TIL	STR	TOT	BCC	BTC	r_{ef}
DVS	−6.4	2.3	−3.1	12.0	4.8	5.1	4.0	178
	(−7.2)	(9.9)	(−5.4)	(13.5)	(10.8)	(13.9)	(4.9)	(176)
MS	−0.9	4.5	−5.6	2.8	0.8	2.9	0.6	218
	(−3.1)	(4.3)	(−5.5)	(3.0)	(−1.3)	(3.6)	(1.4)	(206)
DCS	−0.7	2.3	−1.1	−1.9	−1.4	−0.6	0.3	207
	(−1.6)	(1.9)	(−3.2)	(2.1)	(−0.4)	(1.1)	(1.2)	(203)

NL-SWVs maintained for less than 36 h. Therefore, precipitation is a necessary condition for the longevity of the SWV. It should be noted that these 30 long-lived SWVs all triggered torrential rainfall, and some caused flash floods over the YRB. Additionally, 9 cases of the 30 long-lived SWVs (30%) moved out of the Sichuan Basin. However, of the 139 SWVs that maintained longer than 12 h, less than 20% move out of the Sichuan Basin.

3.2. Vorticity budget of the long-lived SWVs

Vorticity budget at 700 hPa was used to investigate the evolution mechanisms of SWVs. To conduct representative studies, three typical stages were defined, including the developing stage (DVS) that is the time average of vortex initiation and 6 h after the initiation; the maintaining stage (MS) that is the time average of consecutive 12 h in the mid-lifetime of the SWV; and the decaying stage (DCS) that is the time average of vortex dissipation and 6 h before dissipation.

During DVS of the PN-SWV, TOT favored development of the vortex (Table II). From Figure 2(a), vorticity enhanced intensely in the sector from 30° to 130° (counterclockwise, hereinafter the same), due mainly to STR (Figure 2(g)) that is closely related to convergence. An additional rapidly developing region appeared around the circumference from 300° to 330°, mainly due to STR and VAV (Figure 2(g) and (m)), implying that the vertical transport of vorticiy also favored the vortex's development. However, the vorticity around the circumference from 160° to 220° weakened rapidly because of negative TIL and HAV (Figure 2(g) and (m)), which indicates that the tilting effect and horizontal transport of vorticity were detrimental within this region. For the PL-SWV, TOT was much more intense than that of the PN-SWV (Table II), indicating that the PL-SWV developed at a much higher speed. Two rapidly developing areas appeared (Figure 2(d)): the first, in the sector from 300° to 0°, was due mainly to TIL and VAV (Figure 2(j) and (p)), and the second, in the sector of 110°–150°, was due mainly to STR and VAV.

During MS, distributions of all terms changed significantly (Figure 2), implying that main mechanisms accounting for the vortex's evolution differed remarkably from those during DVS. For the PN-SWV, conditions were conducive to sustaining the positive vorticity around the circumference of 30°–60°, 90°–140°, 220°–240°, and 310°–0° (Figure 2(b)), whereas regions along 70° and 180°, as well as the circumference of 250°–300°, mainly featured a reduction in positive vorticity. Overall, TOT was conducive to the maintenance of the PN-SWV (Table II), the vertical transport of vorticity was dominant (Figure 2(n)), and STR was also favorable (Figure 2(h)). For the PL-SWV, positive vorticity within the eastern part of the vortex generally enhanced through convergence and vertical transport (Figure 2(k) and (q)). However, vorticity in the sector of 110°–210° weakened rapidly mainly because of negative STR and TIL (Figure 2(k)) that were determined by divergence and tilting effects. Overall, TOT acted to reduce positive vorticity of the PL-SWV (Table II), implying that this type began to weaken during MS.

During DCS, negative TOT dominated the PN-SWV (Table II), which acted to weaken the vortex. Two strong negative TOT centers appeared in sectors 110°–160° and 270°–320° (Figure 2(c)), mainly due to TIL and STR, respectively (Figure 2(i)). Vertical transport of vorticity acted mainly to slow the attenuation of the vortex (Table II), particularly in the sector from 330° to 30° (Figure 2 (c) and (o)). For the PL-SWV, overall, TOT acted to weaken the vortex (Table II). The negative sector of 10°–130° was determined by negative TIL and HAV (Figure 2(l) and (r)), which was closely related to the tilting effect and horizontal transport of vorticity. The negative sector of 170°–290° was due mainly to negative STR (Figure 2 (l)) that was determined by divergence. Additionally, conditions in the sector of 300°–0° still favored maintenance of the PL-SWV (Figure 2(f)) due mainly to STR (Figure 2(l)) that was determined by convergence.

3.3. Energy conversion characteristics of the long-lived SWVs

Energy conversion associated with the rotational wind KE is effective to describe energy features of vortices. The energy budget was conducted to all long-lived SWVs, and typical stages of the PN- and PL-SWVs were composed respectively under the normalized polar coordinate.

During DVS, positive BTC dominated the PN-SWV (Figure 3(a)). Thus, rotational wind enhanced rapidly through the conversion from divergent wind KE, and this provided favorable energy conditions for the vortex's development. Two positive BTC centers appeared: the first was in the sector of 330°–30° and the second was in the sector of 110°–160°. Positive BCC associated with the release of APE also dominated the PN-SWV (Figure 3(a)), with a center appearing in the sector of 330°–40°; this was very favorable for enhancement of the divergent wind KE that can convert to the rotational wind KE. For the PL-SWV, positive BCC and BTC also dominated the vortex (Figure 3(d)), and they were stronger than those of the PN-SWV, indicating that the PL-SWV developed more rapidly. Strong positive BTC occurred mainly along the circumference from 270° to 210°, and the positive BCC center was located mainly in the central northern part of the vortex (Figure 3(d)).

During MS, for both PN- and PL-SWVs, the distribution of BCC and BTC differed remarkably from those during DVS (Figure 3), indicating that the energy conditions changed significantly. Moreover, the intensity of BCC and BTC both weakened significantly (Table II). Thus, the SWV varied moderately during MS. For the PN-SWV, BTC mainly favored the sustainment of rotational wind in the sector of 230°–60° (Figure 3(b)), whereas it worked conversely in the

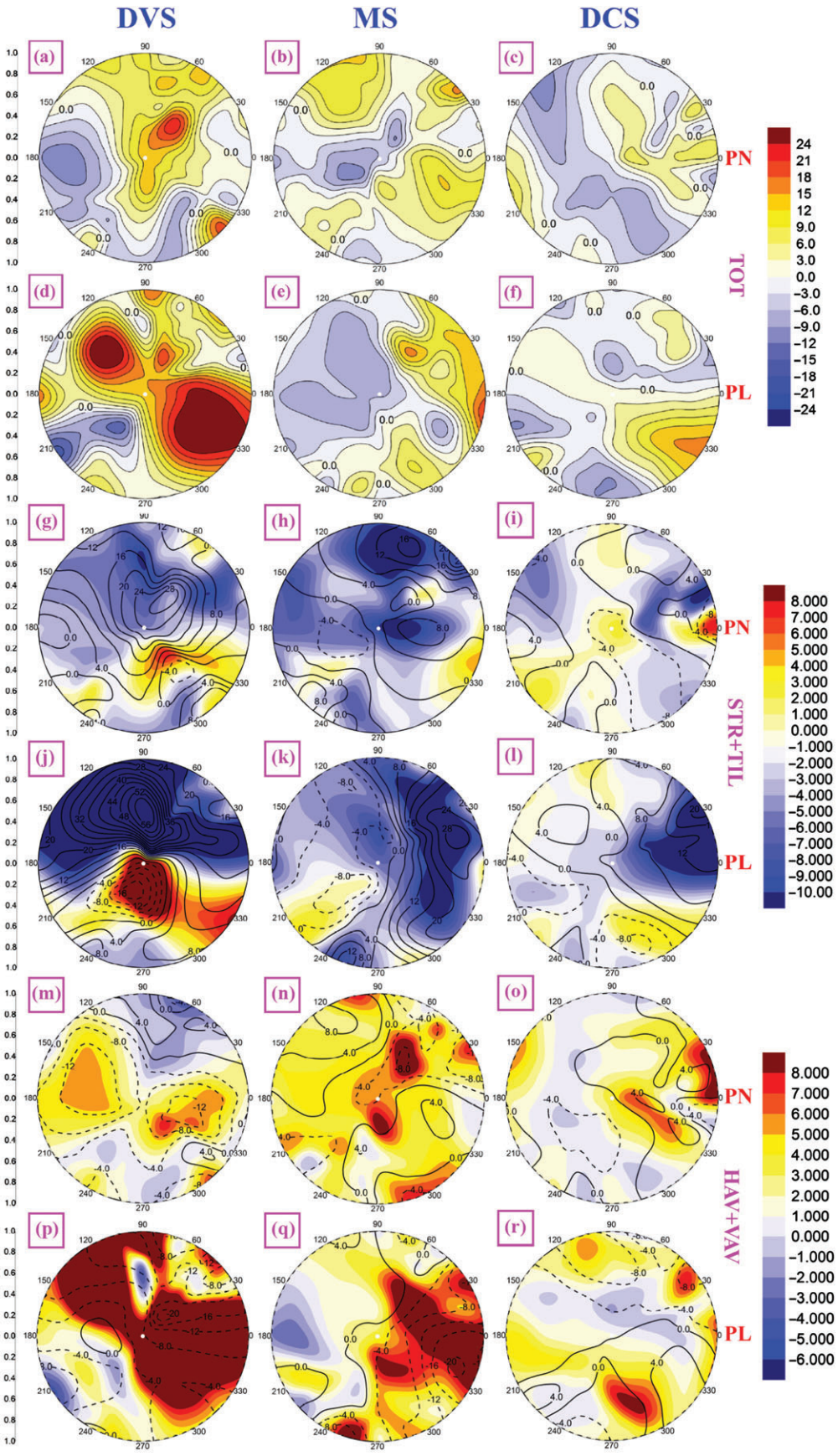

Figure 2. Normalized vorticity budget terms at 700 hPa during the DVS, MS, and DCS of the composed SWV (units: 10^{-10} s^{-2}). Panels (a)–(c) show TOT of the composed PN-SWV, and panels (d)–(f) show TOT of the composed PL-SWV. Panels (g)–(i) show STR (black lines) and TIL (shading) of the composed PN-SWV, and panels (j)–(l) are the same as (g)–(i) but for the composed PL-SWV. Panels (m)–(o) show HAV (black lines) and VAV (shading) of the composed PN-SWV, and panels (p)–(r) are the same as (m)–(o) but for the composed PL-SWV.

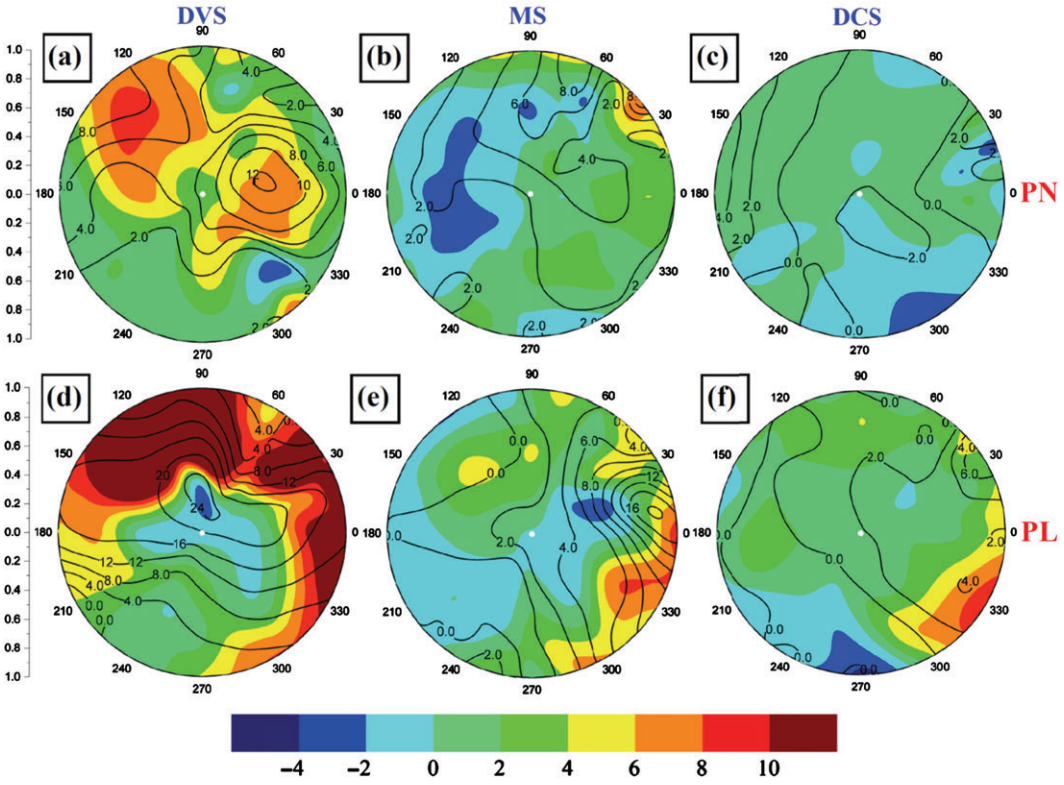

Figure 3. Normalized BCC (black solid lines) and BTC (shading) at 700 hPa (units: 10^{-4} W kg^{-1}) during the DVS (a), MS (b), and DCS (c) of the composed PN-SWV. Panels (d)–(f) are the same as (a)–(c) but for typical stages of the composed PL-SWV.

sector of 120°–230°. BCC still favored the maintenance of divergent wind, with its positive centers mainly around the circumference of 30°–90° (Figure 3(b)). For the PL-SWV, positive BTC that favored sustainment of the rotational wind appeared mainly around the circumference from 270° to 160° (Figure 3(e)). Overall, PL-SWV (Table II) was characterized by release of APE, with positive BCC centers locating mainly around the circumference from 330° to 30°, whereas negative BCC regions appeared mainly around the circumference of 110°–220° (Figure 3(e)) corresponding to the conversion from divergent wind KE to APE.

During DCS of the PN-SWV, BTC mainly favored the maintenance of rotational wind in the sector of 340°–200° (Figure 3(c)), whereas it acted conversely in the sector of 240°–330°. In the middle of the vortex, divergent wind KE generally converted into APE; whereas around the circumference of 90°–220°, 240°–270°, and 340°–40°, the release of APE favored the enhancement of divergent wind. For the PL-SWV, positive BTC still dominated the vortex (Table II), which slowed down the attenuation of the SWV. Around the circumference of 200°–280° (Figure 3(f)), rotational wind generally converted into divergent wind, which might accelerate the vortex's attenuation. The release of APE weakened significantly (Table II), and it was located mainly in the sector of 300°–120°. Negative BCC located mainly in the sector of 180°–290° (Figure 3(f)) acted to reduce the divergent wind.

3.4. Quadrant-averaged features of long-lived SWVs

The evolution of long-lived SWVs was characterized by significant unevenness (Figures 2 and 3), with some quadrants of the vortex developing/dissipating at a much higher speed. Four equal quadrants (Q1–Q4) were defined (Q1: 0°–90°; Q2: 90°–180°; Q3: 180°–270°; Q4: 270°–360°), and the quadrant-averaged budgets were used to describe the unevenness.

During DVS, the PN-SWV enhanced most rapidly in Q1, whereas Q4 was the fastest for PL-SWV (Figure 4(a)). During MS, the PL-SWV began to weaken (Table II), and the weakening within Q2 was the most rapid. For the PN-SWV, weakening was only detected in Q3 (Figure 4(a)). During DCS, both the PN- and PL-SWV weakened (Table II), and the PN-SWV weakened much more rapidly. Q2–Q4 of the PN-SWV and Q1–Q3 of the PL-SWV featured rapid weakening (Figure 4(a)).

Unevenness was also a remarkable feature for the energy conversions associated with long-lived SWVs. During DVS, BTC, and BCC within Q1–Q2 were stronger than those within Q3–Q4 for all long-lived SWVs (Figure 4(b) and (c)). Thus, the energy conditions within Q1–Q2 were more favorable for the SWVs' rapid development. During MS of PL-SWVs, BTC maximized in Q4 and minimized in Q3; BCC also minimized in Q3 but maximized in Q1 (Figure 4(b) and (c)). For the PN-SWVs, BTC maximized in Q1 and minimized in Q2; BCC also maximized in Q1 but

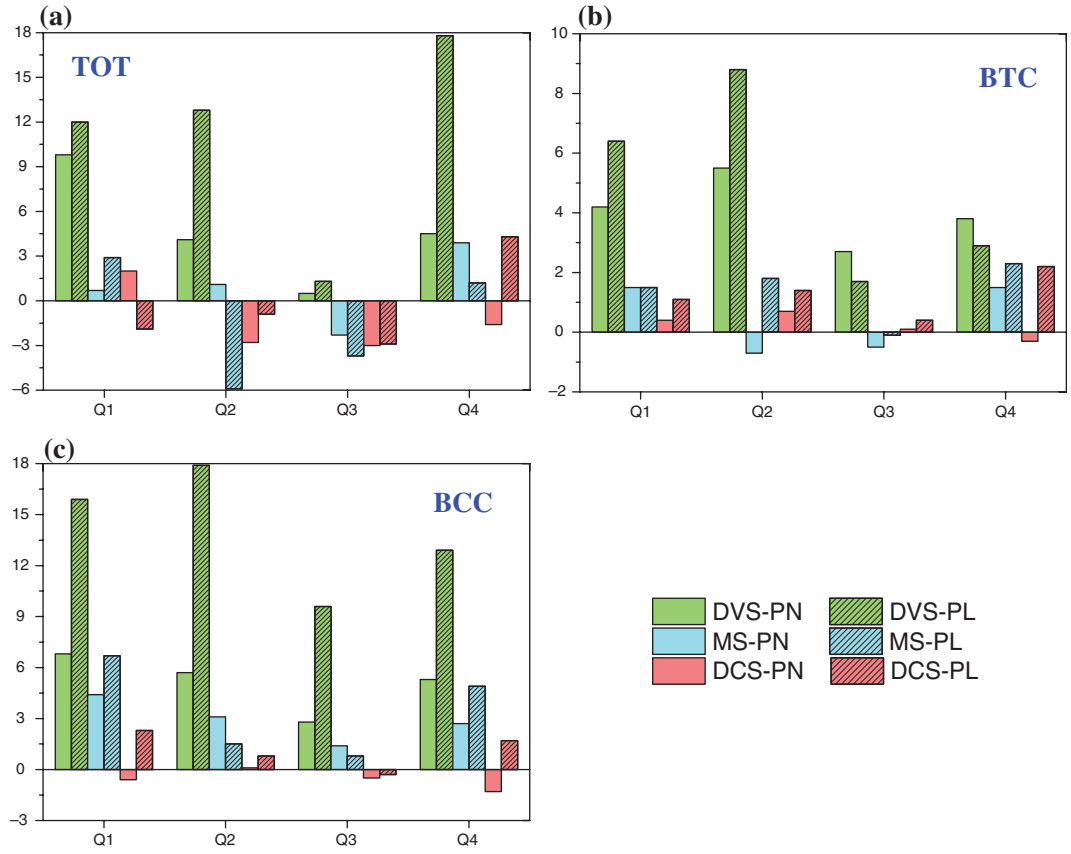

Figure 4. Quadrant-averaged TOT (units: 10^{-10} s^{-2}) (a), BTC (units: 10^{-4} W kg^{-1}) (b), and BCC (units: 10^{-4} W kg^{-1}) (c) during the DVS, MS, and DCS of the composed PN and PL-SWVs.

minimized in Q3. During DCS, BTC and BCC of the PN-SWVs minimized in Q4, whereas for PL-SWVs, they minimized in Q3 (Figure 4(b) and (c)).

4. Concluding remarks

This study is the first analysis of SWVs based on high-resolution reanalysis data ($0.5° \times 0.5°$), which is necessary for accurate detection of SWVs. Also, this study is the first work that reveals the three-dimensional shape, universal evolution mechanisms, and energy features of the long-lived SWVs. Compared with previous studies based on 12-hourly/24-hourly soundings (Chen *et al.*, 2007), more SWVs are detected, and this may render a more comprehensive understanding of the SWVs. Moreover, the new criteria for the SWV classification and the composite method under a normalized polar coordinate turn out to be effective in the SWV study.

Precipitation is a necessary condition for the longevity of the SWV, and the evolution mechanisms and energy features of long-lived SWVs were characterized by significant unevenness, with some quadrants developing/dissipating more rapidly than others. For long-lived SWVs, mechanisms accounting for the development and attenuation differed obviously for the PN- and PL-SWV, whereas the maintaining mechanisms were very similar (Table II). Energy features of long-lived PN- and PL-SWVs were mainly characterized by strong baroclinity and BTC during DVS, moderate baroclinity and weak BTC during MS, and both weak baroclinity and BTC during DCS. BCC was more intense than BTC during the DVS and MS, implying that the release of APE was very conducive to the development and sustainment of long-lived SWVs. Additionally, for those small features at the outskirts of the energy composites, they are closely related to neighboring systems. But it is really hard to evaluate to what extent they are determined by the neighboring systems.

Acknowledgements

The authors thank the NCEP and the CMA for providing the data. Sincere thanks are also extended to Dr Irina Rudeva for the normalized polar coordinate method. The authors also thank Editor Andrew Russell and three anonymous reviewers for their valuable suggestions. This research was supported by the National Key Basic Research and Development Project of China (2012CB417201) and the National Natural Science Foundation of China (41205027, 41375053, and 41275051).

References

Chen QZ, Huang YW, Wang QW, Tan ZM. 2007. The statistical study of the southwest vortices during 1990–2004. *Journal of Nanjing University (Natural Sciences)* **43**: 633–642.

Ding YH, Liu YZ. 1985. On the analysis of typhoon kinetic energy. Part II: Conversion between divergent and nondivergent wind. *Science in China. Series B* **11**: 1045–1054.

Fu SM, Sun JH, Zhao SX, Li WL. 2011. The energy budget of a southwest vortex with heavy rainfall over South China. *Advances in Atmospheric Sciences* **28**: 709–724, doi: 10.1007/s00376–010–0026–z.

Fu SM, Yu F, Wang DH, Xia RD. 2013. A comparison of two kinds of eastward–moving mesoscale vortices during the mei–yu period of 2010. *Science China Earth Sciences* **56**: 282–300, doi: 10.1007/s11430–012–4420–5.

James EP, Johnson RH. 2010. Patterns of precipitation and mesolow evolution in midlatitude mesoscale convective vortices. *Monthly Weather Review* **138**: 909–931, doi: 10.1175/2009MWR3076.1.

Kirk JR. 2003. Comparing the dynamical development of two mesoscale convective vortices. *Monthly Weather Review* **131**: 862–890, doi: 10.1175/1520–0493(2003)131<0862:CTDDOT>2.0.CO;2.

Kuo YH, Cheng LS, Bao JW. 1988. Numerical simulation of the 1981 Sichuan flood. Part I: Evolution of a mesoscale southwest vortex. *Monthly Weather Review* **116**: 2481–2504.

Lu JH. 1986. *Generality of the Southwest Vortex*. China Meteorological Press: Beijing; 270 pp.

Orlanski I. 1975. A rational subdivision of scales for atmospheric processes. *Bulletin of the American Meteorological Society* **56**: 527–530.

Rudeva I, Gulev SK. 2007. Climatology of cyclone size characteristics and their changes during the cyclone life cycle. *Monthly Weather Review* **135**: 2568–2587, doi: 10.1175/MWR3420.1.

Rudeva I, Gulev SK. 2011. Composite analysis of North Atlantic extratropical cyclones in NCEP–NCAR reanalysis data. *Monthly Weather Review* **139**: 1419–1446, doi: 10.1175/2010MWR3294.1.

Saha S, Moorthi S, Pan HL, Wu XG, Wang JD, Nadiga S, Tripp P, Kistler R, Woollen J, Behringer D, Liu HX, Stokes D, Grumbine R, Gayno G, Wang J, Hou YT, Chuang HY, Juang HMH, Sela J, Iredell M, Treadon R, Kleist D, Delst PV, Keyser D, Derber J, Michael E, Meng J, Wei HL, Yang RQ, Lord S, Dool HVD, Kumar A, Wang WQ, Long C, Chelliah M, Xue Y, Huang BY, Schemm JK, Ebisuzaki W, Lin R, Xie PP, Chen MY, Zhou ST, Higgins W, Zou CZ, Liu QH, Chen Y, Han Y, Cucurull L, Reynolds RW, Rutledge G, Goldberg M. 2010. The NCEP climate forecast system reanalysis. *Bulletin of the American Meteorological Society* **91**: 1015–1057, doi: 10.1175/2010BAMS 3001.1.

Tao SY. 1980. *Rainstorms in China*. Science Press: Beijing; 225 pp.

Yang YM, Gu WL, Zhao RL, Liu J. 2010. The statistical analysis of low vortex during Meiyu season in the lower reaches of the Yangtze. *Journal of Applied Meteorological Science* **21**: 11–18.

Zhao SX, Tao ZY, Sun JH, Bei NF. 2004. *Study on Mechanism of Formation and Development of Heavy Rainfalls on Meiyu Front in Yangtze River*. China Meteorological Press: Beijing; 282.

